Searching for intra-cloud positive leaders in VHF

O. Scholten[1,2], B. M. Hare[1,3], J. Dwyer[4], N. Liu[4], C. Sterpka[4], K. Mulrey[5], S. ter Veen[3]

[1]University Groningen, Kapteyn Astronomical Institute, Landleven 12, 9747 AD Groningen, The Netherlands
[2]Interuniversity Institute for High-Energy, Vrije Universiteit Brussel, Pleinlaan 2, 1050 Brussels, Belgium
[3]Netherlands Institute of Radio Astronomy (ASTRON), Postbus 2, 7990 AA Dwingeloo, The Netherlands
[4]Department of Physics and Space Science Center (EOS), University of New Hampshire, Durham NH 03824 USA
[5]Department of Astrophysics/IMAPP, Radboud University Nijmegen, P.O. Box 9010, 6500 GL Nijmegen, The Netherlands

Key Points:

- The intensity in VHF of a intra-cloud positive leader is many orders of magnitude smaller then some cloud-to-ground positive leaders.
- The upper limit of the spectral energy density of the tip of an intra-cloud positive leader is $F = 0.5$ pJ/MHz at 60 MHz, per 100 ns or 5 μW/MHz.
- Our observations support the hypothesis that intra-cloud positive leaders propagate continuously.

Corresponding author: Olaf Scholten, O.Scholten@rug.nl

Abstract

We have used the LOw-Frequency ARray (LOFAR) to search for the growing tip of an intra-cloud (IC) positive leader. Even with our most sensitive beamforming method, where we coherently add the signals of about 170 antenna pairs, we were not able to detect any emission from the tip. Instead, we put constraints on the emissivity of very-high frequency (VHF) radiation from the tip at 0.5 pJ/MHz at 60 MHz, integrated over 100 ns. The limit is independent on whether this emission is in the form of short pulses or continuously. We conclude that IC positive leaders propagate in a continuous process which is in sharp contrast to what is seen to the step-wise propagation seen in some cloud-to-ground positive leaders and for all negative leaders.

1 Introduction

The detection of emitted VHF radio waves is an efficient method to image the development of a lightning discharge since VHF is virtually not attenuated in the atmosphere and thus not obscured by clouds. This thus allows for studying the complete development of the discharge. While VHF is very efficient in detecting negative discharges, the detection of positive discharges has proven to be much more difficult. Except for a few cases such as when positive leaders that propagate to ground (Kong et al., 2008; Wang et al., 2016; Pu et al., 2021), emitted from a tall building (Wang et al., 2016; Visacro et al., 2017), or occur in rocket-triggered lightning (Idone, 1992) they elude direct detection by VHF. If at all, inter and intra cloud positive leaders show in VHF-images only indirectly through small scale discharges, known as needles, along their tracks (Hare et al., 2019; Wu et al., 2019; Pu & Cummer, 2019; Hare et al., 2021) or through dart (sometimes called recoil or K-change) leaders (Jensen et al., 2021).

From a large number of observations we know that positive leaders show in VHF very differently from negative leaders. The growing tips of negative leaders are clearly visible by the copious amounts of VHF emitted due to their step-wise propagation. Newly formed positive leaders can sometimes be traced by intermittent VHF emission along their track, often followed by a dart leader that may propagate all along the track towards the negative leader at the other end. These intermittent VHF emission along the track, by their nature, cannot be the growing tip of the positive leader even though the furthest point where this emission is observed moves up along the track, be it in large jumps (Hare et al., 2019; Wu et al., 2019; Hare et al., 2021). The growing tip of the positive leader must be some distance ahead and the observed VHF emission. To find the tip one thus should search along the positive leader track before the time the track becomes observable by the needle activity (intermittent VHF emission) or by a dart leaders. How much earlier is however not known and is an issue of much interest. To do so we have performed a highly directed search for this tip using the LOw-Frequency ARray (LOFAR) (van Haarlem et al., 2013) since, by coherently adding the signals of about 170 antenna pairs it this offers the most sensitive VHF based lightning-imaging method to date.

In this work we concentrate on one particular section of a rather long positive leader track where we search for evidence of the growing tip all along the track in a few different time windows. The time periods are selected to have a minimum activity elsewhere in the discharge thus to be able to reach the highest possible sensitivity. The present flash is one of the few where periods can be found without a VHF-loud propagating negative leader while a lightning discharge is still in progress. In spite of the high sensitivity we have not been able to locate the tip and have instead set limits on its VHF brightness.

Since this is a highly non-standard analysis we elaborate the followed procedure rather extensively in Section 3. First the part of the flash is discussed, emphasizing the section of the positive leader that is of interest. This is followed by a discussion of the basis of the statistical approach used to determine the upper limit of the intensity. In performing this study we stumble upon a source that is re-ignited, however without any

visible VHF activity within a time span of 0.15 ms before or after anywhere within a distance of 100 m.

In general any varying current (or accelerating charge) will emit electromagnetic radiation. The emission is most intense when the time scale of the variation (or acceleration) is commeasuring with the oscillation frequency of the radiation. This explains why negative leaders are very VHF loud. From the non-observation of VHF from the positive leaders one thus has to conclude that they propagate in a very gradual, continuous mode, completely contrary to the stepping process seen for negative leaders. This conclusion agrees with observations of positive leaders is large-gap discharges (Lalande et al., 2002).

2 Data

For this work we use a 1.5 second LOFAR recording from lightning flashes that occurred on April 24, 2019 at 19:44:32 UTC, which we label as 19A-1. An complete overview of the flashes in this recording is shown in the Supporting Information.

LOFAR (van Haarlem et al., 2013) is a radio telescope consisting of several thousands antennas spread over much of Europe. For these observations we record the signals of antennas in selected Dutch stations only, for the present work about 170 dual-polarized antennas spread over 34 clusters (called stations), operating in the 30 – 80 MHz VHF-band with base lines up to 100 km. To build images from the observations we use two different procedures. One is using the impulsive imager, described in (Scholten, Hare, Dwyer, Sterpka, et al., 2021), where a time-of-arrival-difference method is used to locate the sources of the VHF pulses. Time of arrival differences are calculated using interferometric cross correlations. In the second imaging method, called TRI-D (Scholten, Hare, Dwyer, Liu, et al., 2021; Scholten et al., 2022), the volume to be imaged is voxelated where for each voxel the beam-formed intensity is calculated for 100 ns sections of the time trace. For beamforming a coherent sum over all antenna traces is made while keeping track of their polarization.

With the TRI-D imager a very complete picture is obtained for all, including weak, sources. With the TRI-D imager it is possible to image weak sources with a sensitivity that reaches below the natural background (Sterpka et al., 2021), due to the galactic background radiation, even for cases where the sources do not produce distinct pulses. The impulsive imager, in contrast, obtains the source location of sources for which the pulses can be identified in (almost) all antennas. Both imaging methods use the signals of all recorded antennas.

Fig. 1 shows subsequent time periods of a section of flash 19A-1 that is the focus for this work. The flash initiated close to (-3.0,-33.9, 5.2) km (indicated by a $\bigotimes$ in Fig. 1) at t=0 ms. Several negative leaders are seen to propagate outward for the initiation point at altitudes below 4.5 km, as well as the positive leader we will investigate at higher altitudes. The early part of the track of the positive leader is visible in Fig. 1a-top panel by the scattered sources at altitudes above 5 km as well as some rather short dart leaders. In Fig. 1b the dart leaders are more visible as the discharge is evolving. Some of these dart leaders, such as the ones around t=100 and 150 ms, start in the positive leader and convert into a negative leader towards their end. As seen in Fig. 1c the dart leaders till t=280 ms convert to negative leaders that curl (in the ground-plane projection) under the track of the positive leader. The later ones feed a negative leader complex north of the initiation site that have been truncated to allow focussing on the section of present interest. The track of the positive leader is most clearly visible from the multiple dart leaders at t=530 to 600 ms. It is seen that the positive leader stretches a long distance south and is still visible in the most southern imaged area of Fig. 1c. The part of the positive leader track that is investigated in this work is indicated by the string of grey

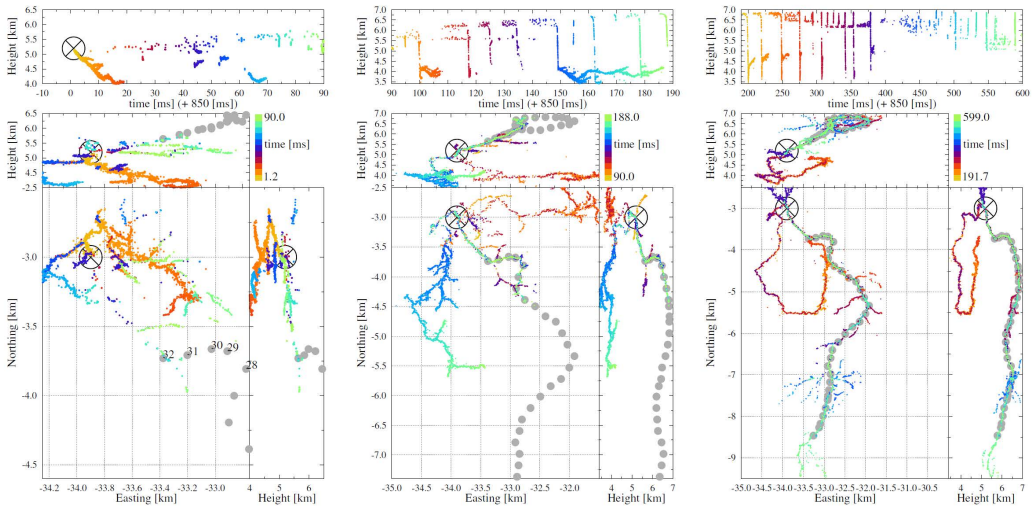

Figure 1: An overview of a series of dart leaders along the track of the positive leader on flash 19A-1 that are of interest for this work. The sub figures have different time and distance scales. The gray circles indicates the track of the positive leader that is investigated in this work where on the left the numbering is given as used later in this work. The ⊗ mark indicates the initiation of the flash.

dots, where the positions of the dots mark the centers of the image cubes where bordering ones just overlap as to give a continuous coverage of the whole track.

3 Results

To search for the growing tip of the positive leaders we use the TRI-D imager since it, by employing beam-form techniques, is able to locate much weaker sources than the impulsive imager and also sources that emit more continuously. The best sensitivity is reached when the VHF background, due to strong VHF sources elsewhere in the flash, is minimal. For flash 19A-1 we selected a few VHF-quiet time periods, most for times between 70 and 83 ms (when needle activity is seen at the base of the positive leader, see Fig. 1a) and two for times around 138.0 ms (when needle activity starts to become visible along the grey-dotted track in Fig. 1b). For each of the selected time we use the TRI-D imager for a period of 0.3 ms to image the possible sources in a sequence of image cubes arranged along the track of the positive leader where no earlier activity was observed and thus where we should expect to find the tip of the positive leader.

To set a limit on the distance the growing tip may have moved from the region where the needle activity is seen, we estimate the propagation velocity of the positive leader. From Fig. 1a it can be seen that in the first 90 ms the VHF-visible portion of the positive leader (i.e. the needles) has grown to a distance of about 1.5 km from the initiation point of the flash indicated by the ⊗ in Fig. 1. From the middle panel it can be seen that in the following 100 ms the needles have appeared along an additional 2 km. Thus, the needles appear along the positive leader channel at a speed of the order of 2×10^4 m/s which is very similar to the estimates found in the literature, see (Gallimberti et al., 2002; Wu et al., 2019; Hare et al., 2021).

On the basis of the estimated speed it seems reasonable to expect that the tip of the positive leader is not more distant from the needle activity than the distance it can travel in 100 ms, thus 2 km. To be conservative, we have searched for the tip over a dis-

tance of 5 km along the dart leader shown in Fig. 1, where the searched track is indicated by the grey dots. In fact, each grey dot marks the center of an image cube of size (200, 180, 250) m located such that their borders just overlap. For each image cube the beam-formed intensity is calculated for the $(100\times120\times50) = 6\times10^6$ voxels of the image cube for all of the 3000 time samples of 100 ns in a 0.3 ms interval centered at a few different times, 5 ms before the start of the flash, ten intervals between 70 and 84 ms, and two around 138 ms after the start of the flash. The length of the voxels in the three directions is reflecting the point-spread function of the system. The first time interval is taken before initiation of this flash to learn about the intensity of the background. The image cubes closest to the initiation point of this flash are placed at the position where needle activity is seen at t=70 till 85 ms.

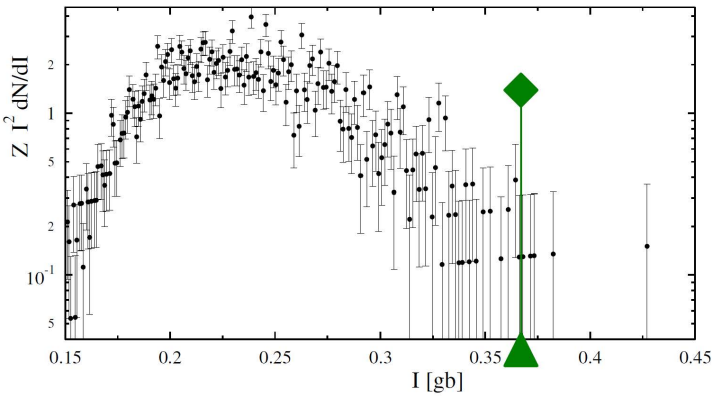

Figure 2: A typical plot showing the normalized number density of sources (multiplied by I^2) as function of the intensity, I (in units [gb], see text) for one image cube over a time span of 0.3 ms. The vertical axis is scaled by I^2 to compensate a generic decrease in source density with intensity. The green line marks the I_5 value (see text) for this tesseract.

In each image cube, following the common procedure for the TRI-D imager, for every time slice of 100 ns, the voxel with maximal intensity is found which is taken as the source location. Each image cube thus yields 3000 source locations and source intensities (at most, since sources at the borders are excluded). A typical intensity distribution for an image tesseract (3-D cube and time) is shown in Fig. 2. In an earlier study it was shown that the intensities spectrum resembles a power law (Machado et al., 2021) and to compensate the strong fall-off at higher intensities the spectrum is multiplied by I^2. A normalization factor $Z^{-1} = \int IdN$ is introduced to make the units dimensionless. Since the total number of sources in a image cube is limited by having at most one source per 100 ns, the number of sources must have a cutoff at smaller amplitudes, which is seen very clearly in Fig. 2. To have a quantitative measure of source strengths we introduce I_N, the intensity for which there are N sources that have an intensity exceeding I_N for a specific tesseract. In Fig. 2 a green marker is placed at the strength $I_5 =$ 0.3670 gb thus marking the point where there are only 5 sources found with a larger intensity.

The intensity of the sources as determined by the TRI-D imager is usually expressed in units of [gb] (Scholten, Hare, Dwyer, Liu, et al., 2021; Sterpka et al., 2021) (see Supporting Information for a more extensive discussion of this unit). A source with strength I gb emits at a spectral energy density, integrated over the full solid angle and over a

time slice Δ_t (fixed to Δ_t=100 ns in this work), of

$$F = 8.5 \times \frac{I}{\text{gb}} \frac{\Delta_t}{100\ \text{ns}}\ \text{pJ/MHz}\ , \tag{1}$$

using a normalization on the background (Mulrey et al., 2019) to determine the relative amounts of instrumental and galactic background.

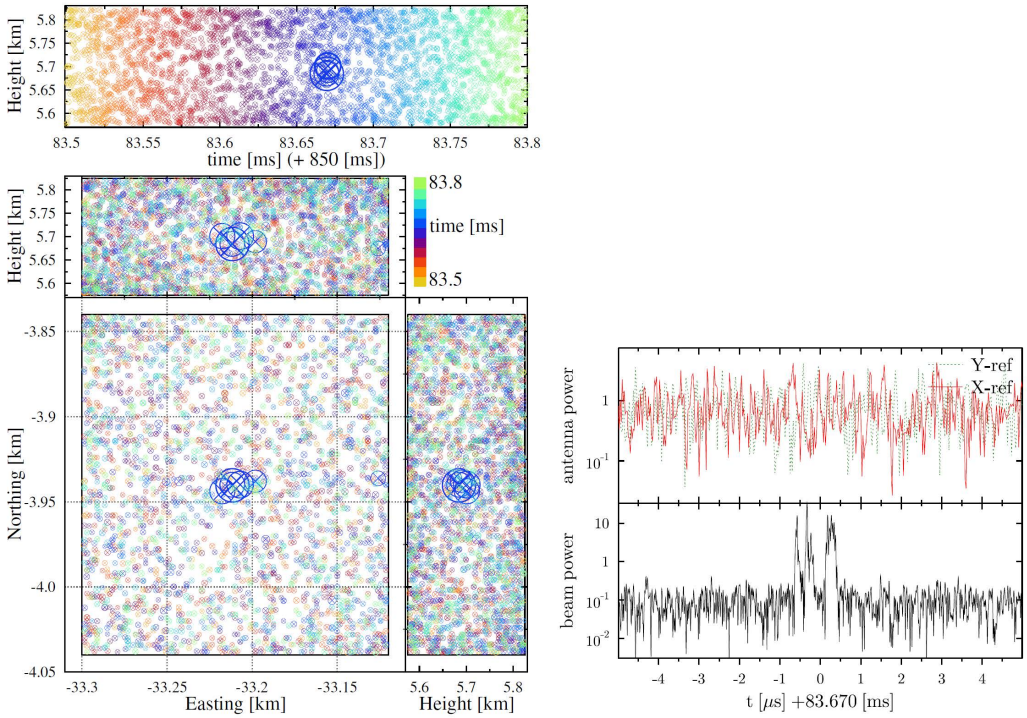

Figure 3: The source that is excluded from the t=83.6 ms time bin. The left shows the TRI-D image is made using an image cube of the same size as in the other analyzes presented in this work. The size of the circles is proportional to the intensity. On the right the power spectrum for an antenna pair in the core of LOFAR is shown in the top panel while the bottom panel shows the beamed spectrum where the signals of 170 antenna-pair have been added coherently for the voxel at the center of the image cube shown to the right where, for display purposes, only 10 μs of the full 0.3 ms spectrum is shown. For each voxel such a spectrum is build.

In performing imaging in the 0.3 ms time interval around t=83.6 ms we noted an increased intensity for the time span 83.665 – 83.675, simultaneously in many different tesseracts, thus excluding it being a genuine source in one of the image cubes. Close investigation revealed that this was due to side beams from a genuine source in the vicinity of the image cubes that was not picked-up by the impulsive imager. This time span was thus excluded from the further search. With the TRI-D imager we succeeded to determine the precise location of this source at (N,E,h)=(-3.94 -33.21 5.7) km as shown in Fig. 3-left with an intensity of about 10 gb. Interesting to note is that this location is the same as that of another source imaged by the impulsive imager at t=81.8 ms, residing on a side branch of the positive leader. The multi-colored background in Fig. 3-left is due to noise sources that are evenly distributed over the image tesseract with an intensity distribution similar to what is shown in Fig. 2. To be able to appreciate the sensitivity of the TRI-D imager the top panel on the right of Fig. 3 shows the power time

trace (square of the amplitude) for the two signals of an antenna pair from the LOFAR core while the bottom shows the coherent sum for the center of the image cube on the left. While in the signal antenna there is hardly any evidence for a pulse it shows in the TRI-D image with an intensity of about 10 gb. The signal power received by an antenna from such a source is determined by the angle dependent gain of the antenna and inversely proportional to the distance of the source to the antenna while the noise background is (almost) constant. A source of 20 gb at 33 km distance is thus hardly visible in the time trace because the antenna gain for a source at a zenith angle of 80° is small. A more extensive discussion is presented in the Supporting Information.

As a signature of the presence of the growing tip of the positive leader we look for excess intensity in the different image tesseracts along the positive leader as compared to what was found as background, i.e. the intensity at 5 ms before the start of the flash. To quantify the intensity we have opted for using I_N with $N = 5$. On the one hand we want N to be small in order to be sensitive to less frequent peaks in VHF emission for the tip but at the same time not too small to limit the influence of statistical fluctuations. If the tip of the positive leader would glow (in VHF) constantly with an intensity of $I_{\rm tip}$ (over each interval of 100 ns in the imaged time interval of 0.3 ms), the intensity spectrum of the sources in the image tesseract containing the tip should show a clear peak at $I_{\rm tip}$ instead of a distribution like shown in Fig. 2, even if $I_{\rm tip}$ were an order of magnitude weaker than the source in Fig. 3. In case that $I_{\rm tip}$ would lie within the bulk of the noise intensities, the presence of the tip, by chance constructive interference with the noise, should increase the high-intensity tail shown in Fig. 2 and thus give rise to a larger I_5 for the tesseract containing the tip as compared to the other tesseracts. These consideration hold even when the growing tip tends to be diffusely emitting length scales of tens of meters.

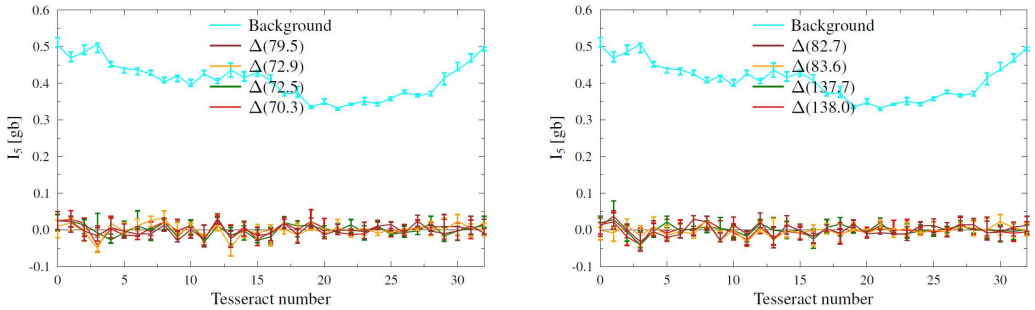

Figure 4: The curve labeled 'Background' gives the I_5 intensities (in [gb]) for successive tesseracts (image cubes calculated for a time-span of 0.3 ms sliced in 100 ns bins) along the track of the positive leader centered around at 5 ms before the flash initiated. The other curves give the difference of the I_5 values for the image cubes at specified times with the background values. The highest tesseract numbers are closest to the base of the positive leader, see Fig. 1a.

The central times for the tesseracts of 0.3 ms duration were chosen such that there is a minimum of sources elsewhere in the discharge that, by virtue of 'side beams', would introduce false sources and thus inadvertently increase the I_5 values. The 32 different locations of the tesseracts were taken as indicated in Fig. 1 where the one with the highest number is nearest to the initiation point. At the earliest instances of the image tesseracts there was needle activity seen at the same spots, but (just) outside the time span covered by the tesseract. This to make sure that propagating tip should be captured in the analysis. The positions of the tesseracts are fixed to a number of specific locations

as the intensities of background-noise sources depends on the location, see Fig. 4. The background values for I_5 at each position are determined by analyzing tesseracts at 5 ms before the flash initiated, making thus sure that there is no positive leader present yet. To give an impression of the statistical significance of the values we give 'error' bars that range from I_3 at the upper to I_7 at the lower end. The earlier times (between t=70.3 ms and 83.6 ms, see Fig. 4) were chosen while there was needle activity seen (see Fig. 1-left). The later times t=137.7 and 138.0 ms were chosen soon after a dart leader was initiated in this positive leader, just before needle activity started again (see the middle panels of Fig. 1). To express the significance we present in Fig. 4 the differences, $\Delta(t) = I_5(t) - I_5(\text{Background})$ for image tesseracts at the identical locations, marked by the numbers given on the horizontal scale in Fig. 4. The 'error' bars on $\Delta(t)$ are the sum of those for $I_5(\text{Background})$ and $I_5(t)$. In Figure S3 in Supporting Information the analysis is shown for another four selected times.

4 Discussion

Fig. 4 shows that the differences in $I_5(t)$ values with the noise floor, $\Delta(t)$, are vanishingly small over a distance of about 5 km from the point where needle activity was seen at times when the positive leader is expected to be propagating. From this it can thus be concluded that either 1) the assumption is wrong and the positive leader is not propagating or that 2) the propagating positive leader is emitting VHF radiation at an intensity that is below our detection limit. We find it highly unlikely that the positive leader has stopped propagating since we see twinkling activity at its base of the positive leader track around the time periods we have investigated. We thus conclude that the tip of the positive leader is extremely VHF quiet while propagating, to the extent that we find no trace of the tip even when using the TRI-D imager under the most favorable conditions.

To set an upper limit of the intensity of the positive leader tip we have argued that $\Delta(t)$ values should be about as large as the VHF-intensity emitted by the tip, I_{tip}. Such an emission should show as peak in Fig. 4 at I_{tip} for the particular tesseract in which the tip is propagating. Additionally, the propagating tip should show as a peak in each curve in Fig. 4, that gradually moves to further distances down the channel for tesseracts at later times. Obviously, this is not seen. One thus can put a conservative limit of 0.05 gb on I_{tip} of this positive leader. Using Eq. (1), this leads to the conclusion that the spectral energy density of the tip at 60 MHz is less than $F = 0.5$ pJ/MHz over a 100 ns slice. Even if the positive leader was propagating in a stepping mode the derived limit is valid as in Refs (Kong et al., 2008; Pu et al., 2021) it is shown that stepped positive leaders show a stepping time ranging from 30 μs down to a fraction of 5 μs. A time interval of 0.3 ms will therefore contain many steps and the derived intensity limit thus should also apply to the case that the IC positive leader is propagating in a stepping mode.

Another evidence for the VHF quietness of the positive leader can be taken from Fig. 3. For about 0.15 ms before and after observing the source there is no detected activity anywhere along the track of the positive leader. At exactly the same spot a source was imaged by the impulsive imager at t=82 ms, see figure S4 in Supporting Information. These sources lie on a side branch of the main positive leader that is about 1 km long (at least the part made visible through dart leaders). As a second test we have repeated the same search for the positive leader tip along this short side branch reaching to the same conclusion as for the main branch. The results of this analysis are presented in the supporting information figures S2 and S3. We see this as another evidence that the positive leader is active at these times while the growing tip remains invisible in VHF.

Our observation that the tip of intra- and inter-cloud positive leaders is extremely quiet in VHF is in stark contrast with the observation (Pu et al., 2021) of a VHF-loud positive leader in a cloud-to-ground (CG) discharge showing clear stepping very simi-

lar to what is seen in optical observations (Willett et al., 1999; Idone, 1992; Kong et al., 2008; Wang et al., 2016; Visacro et al., 2017) of rocket triggered positive leaders and positive leaders emanating from high buildings. Another stark contrast is that the VHF-loud positive leaders propagate at velocities of order 2×10^6 m/s while the one of this work is probably propagating at a speed of only 2×10^4 m/s. Very interesting in this respect is the observation made in (Lalande et al., 2002) that when triggered lightning is propagating to higher altitudes there is a growing continuous current on which oscillations are super imposed that are gradually damped.

These observations suggest that when the positive leader is approaching a well conducting surface, or is well connected to a large conducting body (=Earth) the charge at its tip must be large with an electric field in the streamer zone that surpasses some critical value apparently causing the leader to be impulsive and propagate with a large speed.

Under laboratory conditions, as discussed in (Gallimberti et al., 2002), the positive leader is weakly luminous and shows continuous propagation with a constant glow of streamers at the tip. Its velocity is of order 2×10^4 m/s which suffices to keep the electric field at the tip sufficiently high to sustain the ionization processes in a diffuse corona region. These observations of the propagation speed and the continuous propagation that implies a constant, non varying current (and thus hardly any VHF emission) and consistent with our observations.

5 Summary

We have performed a search for the tip of a positive cloud-to-cloud leader using the TRI-D imager on data from LOFAR. In the process we have been able to set an upper limit of the VHF-emissivity of the tip at 60 MHz of $F = 0.5$ pJ/MHz integrated over 100 ns, or of 5 μW/MHz if emitting continuously.

Our results are consistent with the laboratory observations of a positive leader as discussed in (Gallimberti et al., 2002). A smooth propagation of the corona at the tip is seen, creating the positive leader behind it in a continuous motion. In such a smooth and continuous process no (hardly any) VHF will be emitted which is consistent with our upper limit. In addition the propagation velocities reported in (Gallimberti et al., 2002), 2×10^4 m/s, are the same as what is deduced for natural CC positive leaders.

Open Research Section

The data are available from the LOFAR Long Term Archive (for access see (ASTRON, 2020)), under the following locations:
`L703974_D20190424T194432.504Z_stat_R000_tbb.h5`
all of them with the same prefix
`srm://srm.grid.sara.nl/pnfs/grid.sara.nl/data/lofar/ops/TBB/lightning/`
and where "stat" should be replaced by the name of the station, CS001, CS002, CS003, CS004, CS005, CS006, CS007, CS011, CS013, CS017, CS021, CS024, CS026, CS030, CS031, CS032, CS101, CS103, RS106, CS201, RS205, RS208, RS210, CS301, CS302, RS305, RS306, RS307, RS310, CS401, RS406, RS407, RS409, CS501, RS503, or RS508.
To access this data, please create an account following instructions at (ASTRON, 2020) and follow the instructions for "Staging Transient Buffer Board data". In particular the utility "wget" should be used as in
`wget https://lofar-download.grid.surfsara.nl/lofigrid/SRMFifoGet.py?surl=location`
where "location" is the location specified in the above.

The software used for data analysis is available at (Scholten, 2022).

Figures 1 till 4 in this work have been made using the Graphics Layout Engine (GLE) (Pugmire et al., 2015) plotting package. The data displayed in these figures may be retrieved from (Scholten, 2023).

Acknowledgments

BMH is supported by the NWO [grant number VI.VENI.192.071]and the ERC [Grant No. 101041097].

LOFAR (van Haarlem et al., 2013) is designed and constructed by ASTRON collectively operated by the International LOFAR Telescope (ILT) foundation under a joint scientific policy. The ILT resources have benefitted from the following recent major funding sources: CNRS-INSU, Observatoire de Paris and Université d'Orléans, France; BMBF, MIWF-NRW, MPG, Germany; Science Foundation Ireland (SFI), Department of Business, Enterprise and Innovation (DBEI), Ireland; NWO, The Netherlands; The Science and Technology Facilities Council, UK.

References

ASTRON. (2020). *LOFAR Long Term Archive Access.* https://www.astron.nl/lofarwiki/doku.php?id=public:lta_howto.

Gallimberti, I., Bacchiega, G., Bondiou-Clergerie, A., & Lalande, P. (2002). Fundamental processes in long air gap discharges. *C.R. Physique*, *3*, 1335–1359. Retrieved from https://doi.org/10.1016/S1631-0705(02)01414-7 doi: 10.1016/S1631-0705(02)01414-7

Hare, B. M., Scholten, O., Dwyer, J., Strepka, C., Buitink, S., Corstanje, A., ... Winchen, T. (2021). Needle propagation and twinkling characteristics. *Journal of Geophysical Research: Atmospheres*, *126*(6), e2020JD034252. Retrieved from https://agupubs.onlinelibrary.wiley.com/doi/abs/10.1029/2020JD034252 doi: https://doi.org/10.1029/2020JD034252

Hare, B. M., Scholten, O., Dwyer, J., Trinh, T. N. G., Buitink, S., ter Veen, S., ... Zucca, P. (2019). Needle-like structures discovered on positively charged lightning branches. *Nature*, *568*, 360–363. doi: 10.1038/s41586-019-1086-6

Idone, V. P. (1992). The luminous development of florida triggered lightning. *Journal of Atmospheric Electricity*, *12*(1), 23-28. doi: 10.1541/jae.12.23

Jensen, D. P., Sonnenfeld, R. G., Stanley, M. A., Edens, H. E., da Silva, C. L., & Krehbiel, P. R. (2021). Dart-leader and k-leader velocity from initiation site to termination time-resolved with 3d interferometry. *Journal of Geophysical Research: Atmospheres*, *126*(9), e2020JD034309. Retrieved from https://agupubs.onlinelibrary.wiley.com/doi/abs/10.1029/2020JD034309 doi: https://doi.org/10.1029/2020JD034309

Kong, X., Qie, X., & Zhao, Y. (2008). Characteristics of downward leader in a positive cloud-to-ground lightning flash observed by high-speed video camera and electric field changes. *Geophysical Research Letters*, *35*(5). Retrieved from https://agupubs.onlinelibrary.wiley.com/doi/abs/10.1029/2007GL032764 doi: https://doi.org/10.1029/2007GL032764

Lalande, P., Bondiou-Clergerie, A., Bacchiega, G., & Gallimberti, I. (2002). Observations and modeling of lightning leaders. *C.R. Physique*, *3*, 1375–1392. Retrieved from https://doi.org/10.1016/S1631-0705(02)01413-5 doi: 10.1016/S1631-0705(02)01413-5

Machado, J., Scholten, O., Hare, B., Buitink, S., Corstanje, A., Falcke, H., ... et al. (2021). The relationship of lightning radio pulse amplitudes and source altitudes as observed by lofar. *Earth and Space Science Open Archive*, *n/a*(n/a), e2021EA001958. Retrieved from https://agupubs.onlinelibrary.wiley.com/doi/abs/10.1029/2021EA001958 (e2021EA001958 2021EA001958) doi: https://doi.org/10.1029/2021EA001958

Mulrey, K., Bonardi, A., Buitink, S., Corstanje, A., Falcke, H., Hare, B., ... Winchen, T. (2019). Calibration of the lofar low-band antennas using the galaxy and a model of the signal chain. *Astroparticle Physics*, *111*, 1 - 11. Retrieved from http://www.sciencedirect.com/science/article/pii/

S0927650518302810 doi: https://doi.org/10.1016/j.astropartphys.2019.03.004

Pu, Y., & Cummer, S. A. (2019). Needles and Lightning Leader Dynamics Imaged with 100 – 200 MHz Broadband VHF Interferometry. *Geophysical Research Letters*, *46*(22), 13556-13563. Retrieved from https://agupubs.onlinelibrary.wiley.com/doi/abs/10.1029/2019GL085635 doi: 10.1029/2019GL085635

Pu, Y., Cummer, S. A., & Liu, N. (2021). Vhf radio spectrum of a positive leader and implications for electric fields. *Geophysical Research Letters*, *48*(11), e2021GL093145. Retrieved from https://agupubs.onlinelibrary.wiley.com/doi/abs/10.1029/2021GL093145 (e2021GL093145 2021GL093145) doi: https://doi.org/10.1029/2021GL093145

Pugmire, C., Mundt, S. M., LaBella, V. P., & Struyf, J. (2015). *Graphics layout engine gle 4.2.5 user manual.* https://en.wikipedia.org/wiki/Graphics_Layout_Engine. Retrieved from https://glx.sourceforge.io/index.html

Scholten, O. (2022, December). *Lofar lightning imaging.* Zenodo. Retrieved from https://doi.org/10.5281/zenodo.7393903 (v22.12 of this package) doi: 10.5281/zenodo.7393903

Scholten, O. (2023). *Data for figures 1 till 4 of "Searching for intra-cloud positive leaders in VHF".* Zenodo. Retrieved from https://doi.org/10.5281/zenodo.7655030 doi: 10.5281/zenodo.7655030

Scholten, O., Hare, B. M., Dwyer, J., Liu, N., Sterpka, C., Buitink, S., ... ter Veen, S. (2021, Sep). Time resolved 3d interferometric imaging of a section of a negative leader with lofar. *Phys. Rev. D*, *104*, 063022. Retrieved from https://link.aps.org/doi/10.1103/PhysRevD.104.063022 doi: 10.1103/PhysRevD.104.063022

Scholten, O., Hare, B. M., Dwyer, J., Liu, N., Sterpka, C., Kolmašová, I., ... ter Veen, S. (2022, Mar). Interferometric imaging of intensely radiating negative leaders. *Phys. Rev. D*, *105*, 062007. Retrieved from https://link.aps.org/doi/10.1103/PhysRevD.105.062007 doi: 10.1103/PhysRevD.105.062007

Scholten, O., Hare, B. M., Dwyer, J., Sterpka, C., Kolmasova, I., Santolik, O., ... Winchen, T. (2021). The initial stage of cloud lightning imaged in high-resolution. *Journal of Geophysical Research: Atmospheres*, *126*(4), e2020JD033126. Retrieved from https://agupubs.onlinelibrary.wiley.com/doi/abs/10.1029/2020JD033126 (e2020JD033126 2020JD033126) doi: https://doi.org/10.1029/2020JD033126

Sterpka, C., Dwyer, J., Liu, N., Hare, B. M., Scholten, O., Buitink, S., ... Nelles, A. (2021). The spontaneous nature of lightning initiation revealed. *Geophysical Research Letters*, *48*(23), e2021GL095511. Retrieved from https://agupubs.onlinelibrary.wiley.com/doi/abs/10.1029/2021GL095511 (e2021GL095511 2021GL095511) doi: https://doi.org/10.1029/2021GL095511

van Haarlem, M. P., et al. (2013). LOFAR: The LOw-Frequency ARray. *A&A*, *556*, A2. doi: 10.1051/0004-6361/201220873

Visacro, S., Guimaraes, M., & Murta Vale, M. H. (2017). Features of upward positive leaders initiated from towers in natural cloud-to-ground lightning based on simultaneous high-speed videos, measured currents, and electric fields. *Journal of Geophysical Research: Atmospheres*, *122*(23), 12,786-12,800. doi: 10.1002/2017JD027016

Wang, Z., Qie, X., Jiang, R., Wang, C., Lu, G., Sun, Z., ... Pu, Y. (2016). High-speed video observation of stepwise propagation of a natural upward positive leader. *Journal of Geophysical Research: Atmospheres*, *121*(24), 14,307-14,315. doi: 10.1002/2016JD025605

Willett, J., Davis, D., & Laroche, P. (1999). An experimental study of positive leaders initiating rocket-triggered lightning. *Atmospheric Research*, *51*(3), 189-219. Retrieved from https://www.sciencedirect.com/science/article/pii/

S0169809599000083 doi: https://doi.org/10.1016/S0169-8095(99)00008-3

Wu, T., Wang, D., & Takagi, N. (2019). Velocities of positive leaders in intracloud and negative cloud-to-ground lightning flashes. *Journal of Geophysical Research: Atmospheres*, *124*(17-18), 9983-9995. Retrieved from https://agupubs.onlinelibrary.wiley.com/doi/abs/10.1029/2019JD030783 doi: 10.1029/2019JD030783

Figure 4.

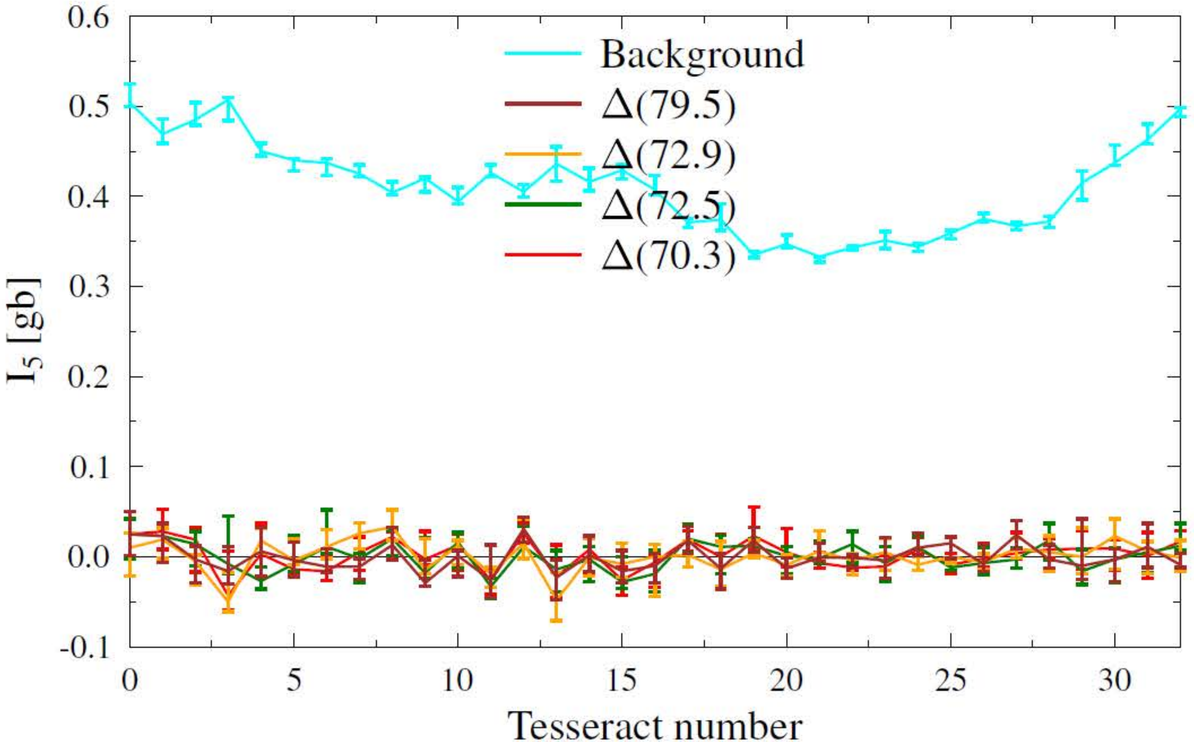
Background
Δ(79.5)
Δ(72.9)
Δ(72.5)
Δ(70.3)
I_5 [gb]
Tesseract number

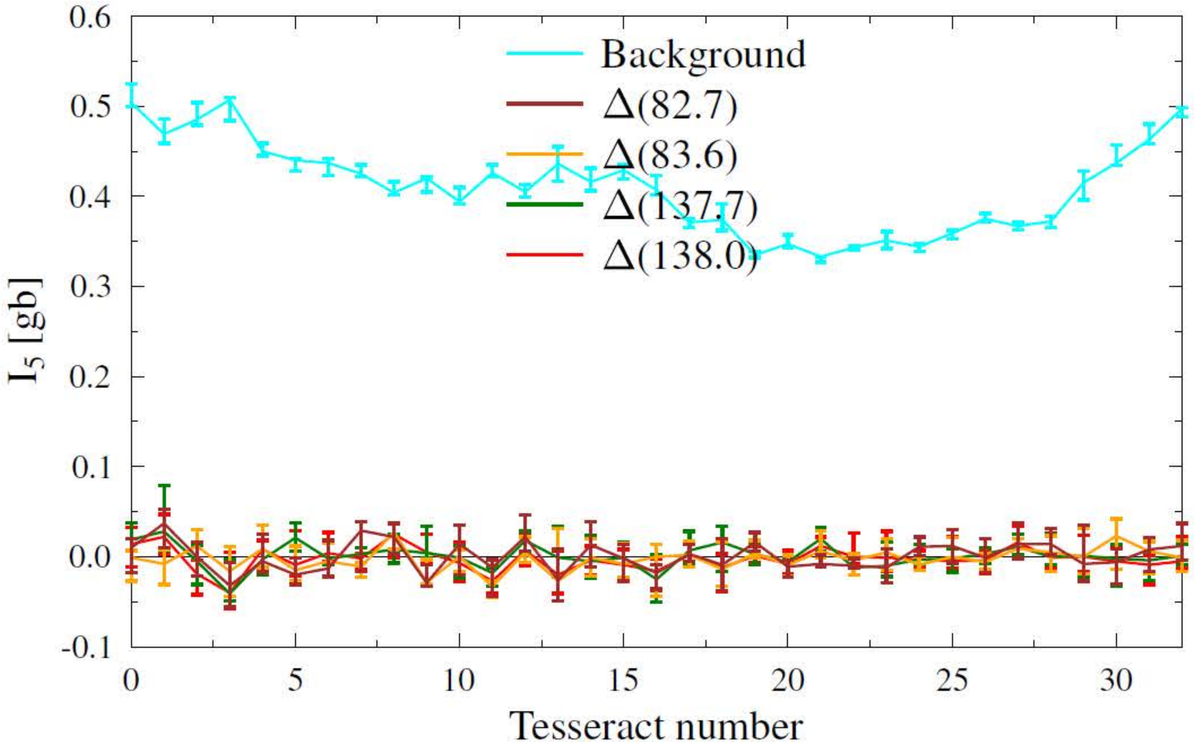
Background
Δ(82.7)
Δ(83.6)
Δ(137.7)
Δ(138.0)
I_5 [gb]
Tesseract number

Figure 3.

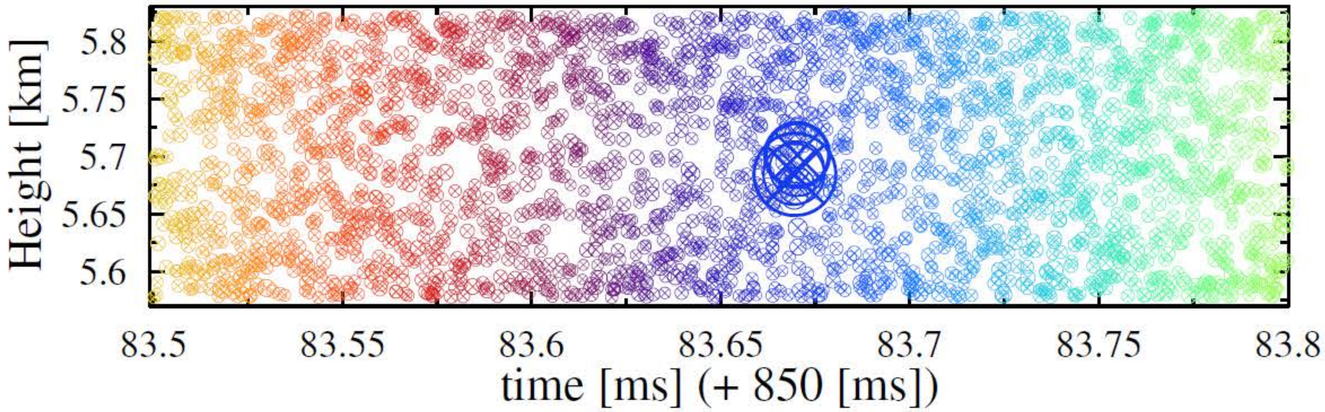
Height [km]
5.8
5.75
5.7
5.65
5.6
83.5
83.55
83.6
83.65
83.7
83.75
83.8
time [ms] (+ 850 [ms])

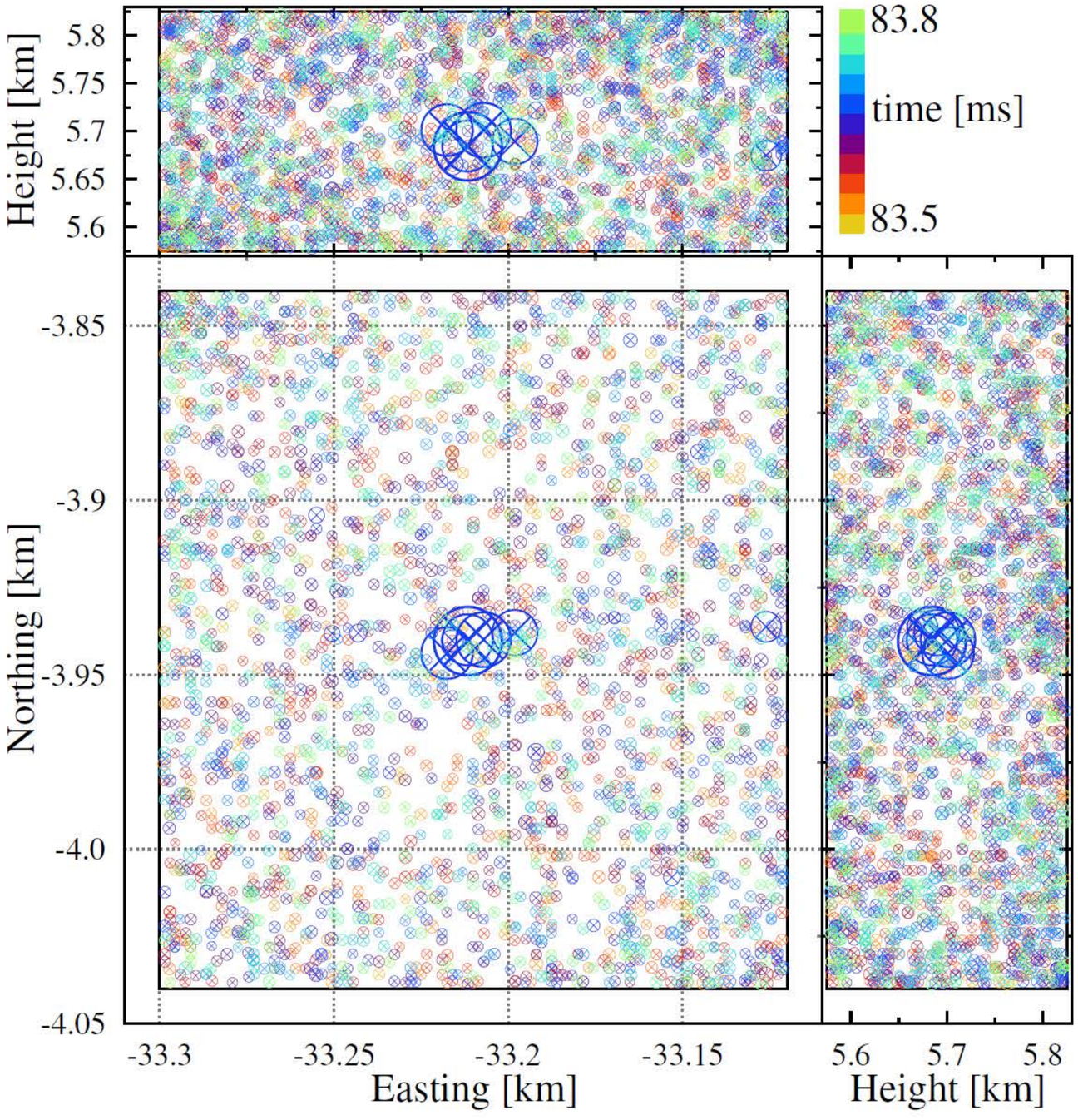
Height [km]
5.8
5.75
5.7
5.65
5.6
83.8
time [ms]
83.5
-3.85
-3.9
-3.95
-4.0
-4.05
Northing [km]
-33.3
-33.25
-33.2
-33.15
Easting [km]
5.6
5.7
5.8
Height [km]

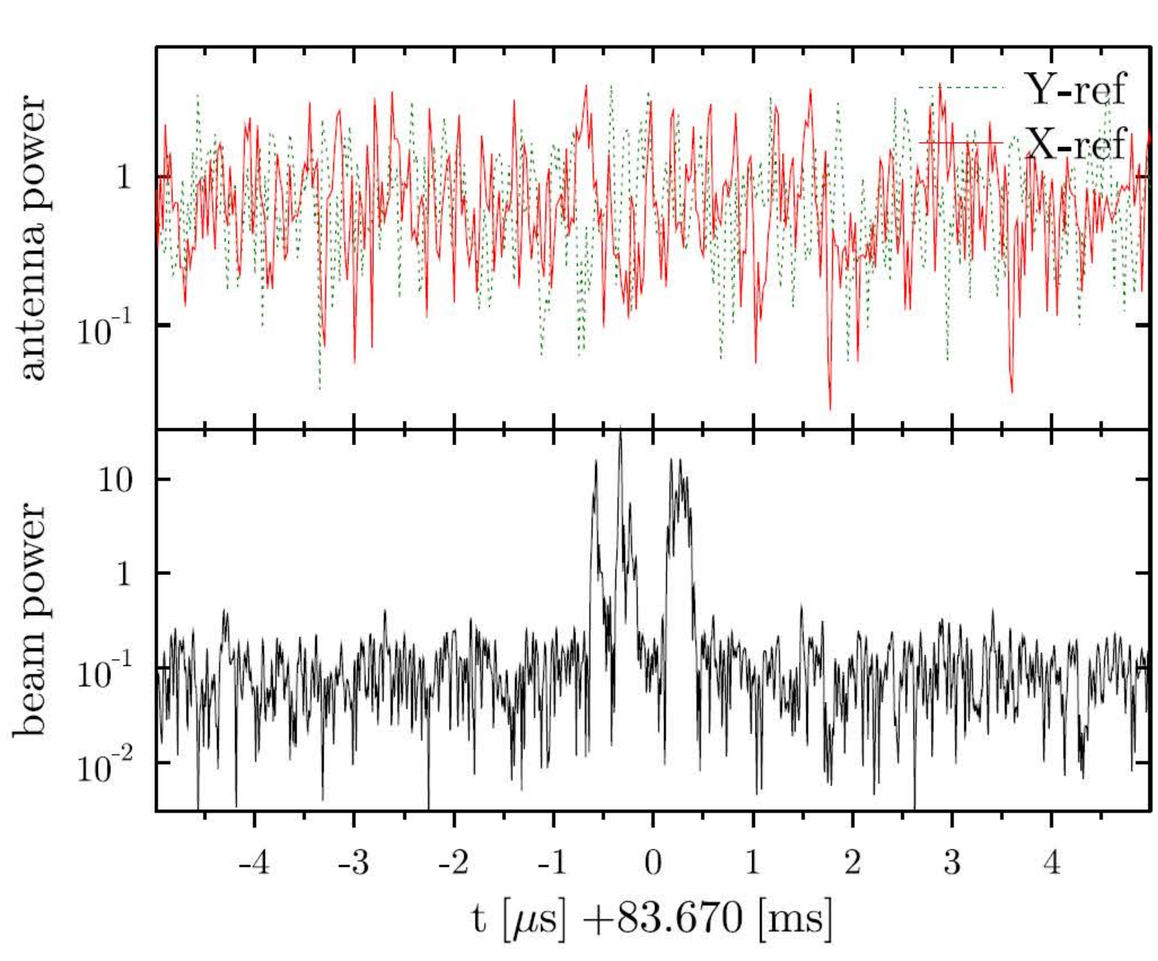
Y-ref
X-ref
antenna power
1
10^{-1}
beam power
10
1
10^{-1}
10^{-2}
-4
-3
-2
-1
0
1
2
3
4
t [μs] +83.670 [ms]

Figure 2.

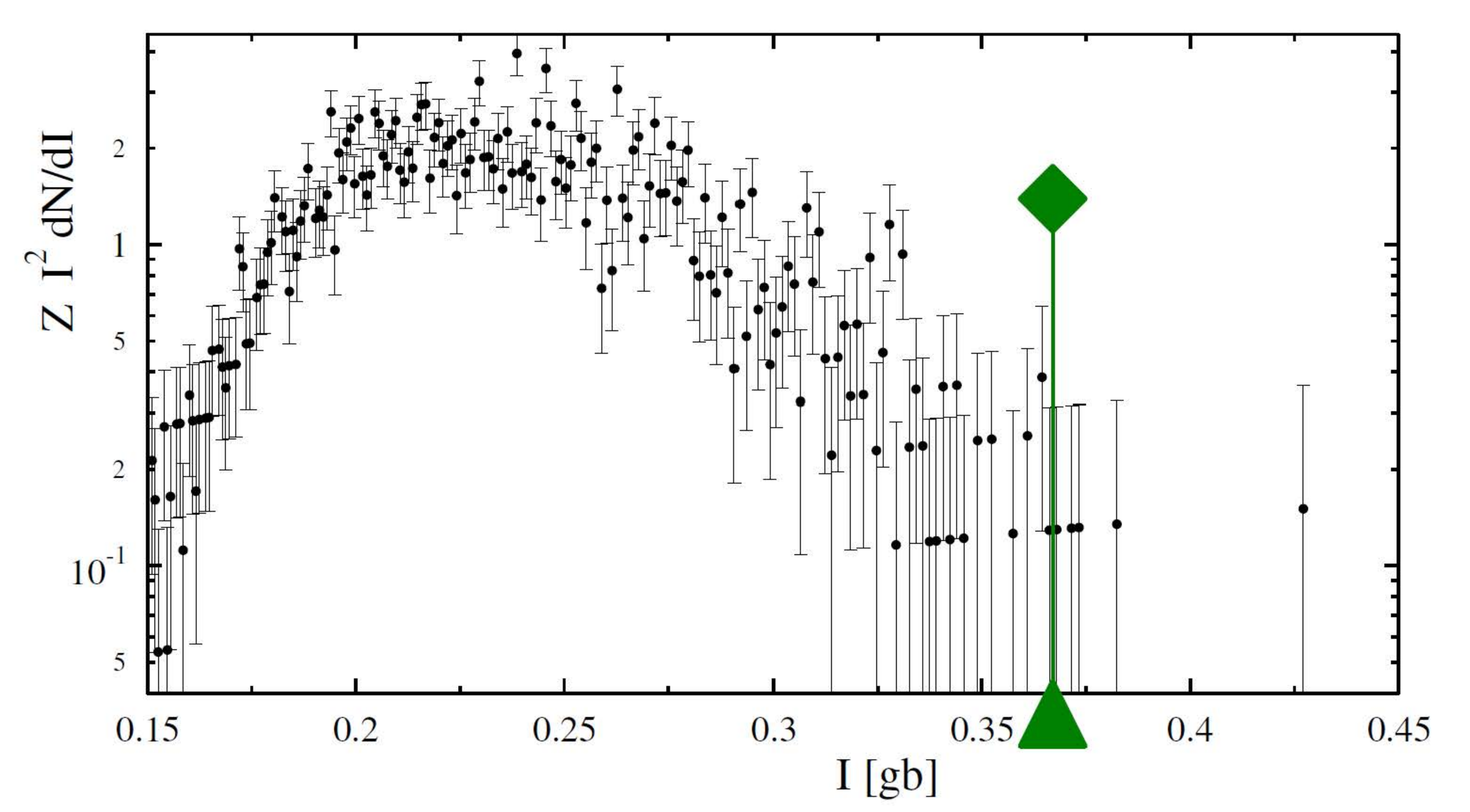
Z I^2 dN/dI
2
1
5
2
10^{-1}
5
0.15
0.2
0.25
0.3
0.35
0.4
0.45
I [gb]

Figure 1.

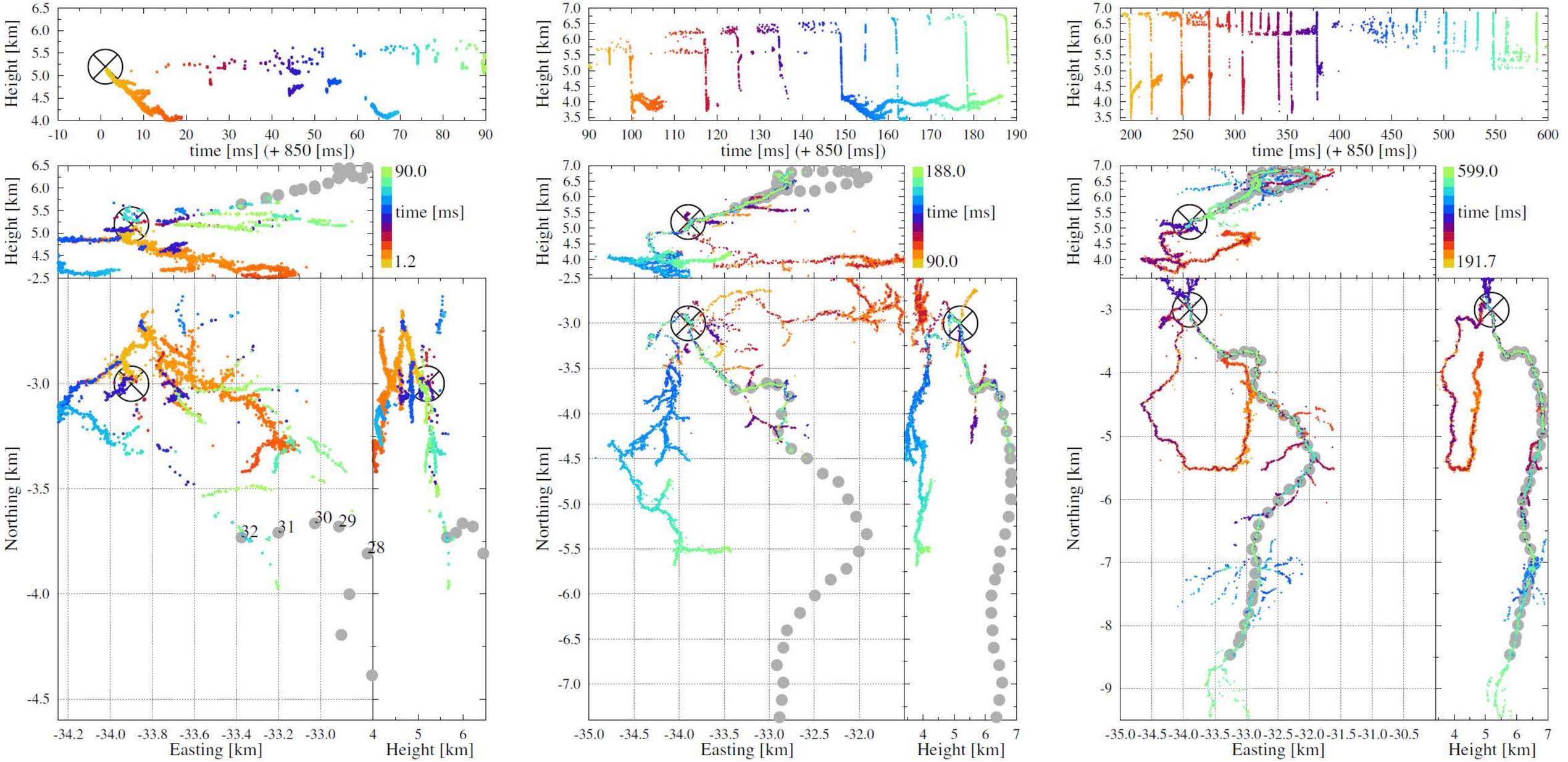
Height [km]
time [ms] (+ 850 [ms])
90.0
time [ms]
1.2
188.0
90.0
599.0
191.7
Northing [km]
Easting [km]
32
31
30
29
28